A Novel Wound Dressing Based on Ag/Graphene Polymer Hydrogel: Effectively Kill Bacteria and Accelerate Wound Healing

Zengjie Fan, Bin Liu, Jinqing Wang, Songying Zhang, Qianqian Lin, Peiwei Gong, Limin Ma, and Shengrong Yang*

Avoiding wound infection and retaining an appropriate level of moisture around woundz are major challenges in wound care management. Therefore, designing hydrogels with desired antibacterial performance and good water-maintaining ability is of particular significance to promote the development of wound dressing. Thus a series of hydrogels are prepared by crosslinking of Ag/graphene composites with acrylic acid and *N*,*N*′-methylene bisacrylamide at different mass ratios. The antibacterial performance and accelerated wound-healing ability of hydrogel are systematically evaluated with the aim of attaining a novel and effective wound dressing. The as-prepared hydrogel with the optimal Ag to graphene mass ratio of 5:1 (Ag5G1) exhibits stronger antibacterial abilities than other hydrogels. Meanwhile, Ag5G1 hydrogel exhibits excellent biocompatibility, high swelling ratio, and good extensibility. More importantly, in vivo experiments indicate that Ag5G1 hydrogel can significantly accelerate the healing rate of artificial wounds in rats, and histological examination reveals that it helps to successfully reconstruct intact and thickened epidermis during 15 day of healing of impaired wounds. In one word, the present approach can shed new light on designing of antibacterial material like Ag/graphene composite hydrogel with promising applications in wound dressing.

1. Introduction

Skin is an important natural barrier organ for protecting internal organs from the external environment and preventing body dehydration,[1] and it would lose its protected mechanism upon damage. If this happens, microorganisms would invade easily and start to form colonies thereby leading to severe wound infection, impeding healing process and even causing life threatening complications.[2] In addition, severe wound dehydration would disturb ideal moist healing environment and delay wound healing.[3] Therefore, substantial efforts are being made to develop new materials for protecting damaged skin from infections and dehydration. For this purpose, traditional dry dressings such as cotton wool, natural or synthetic bandages and gauzes are significant for the initial stages of wound healing, but they are dry and cannot provide a moist environment, while they are also often liable to adhere to desiccated wound surfaces and finally induce trauma upon removal.[4] In order to overcome these drawbacks, researchers, inspired by the concept of moist wound healing, have developed various wet dressings.[5,6] Among them, special attentions have been paid to hydrogels because they can maintain a moist environment at the wound interface, allow gaseous exchange, act as a barrier to microorganisms, remove excess exudates, have excellent biocompatibility, promote a rapid healing of wound, and be easily removed without trauma.[7]

Conventional hydrogels consist of natural or synthetic polymers and usually exhibit relatively poor mechanical properties and small equilibrium-swelling ratio, which limits their practical applications as dressings.[8,9] To deal with this issue, researchers have paid special attention to graphene, a single-layer and two-dimensional lattice with high mechanical strength, big surface area, good thermal and electrical conductivity and excellent biocompatibility.[10–13] This is because, firstly, graphene can be produced from graphene oxide (denoted as GO) in a large-scale and low-cost strategy,[14,15] which facilitates low-cost and large area preparation of graphene hydrogels. Secondly, graphene with high mechanical strength can be used as an efficient filler to enhance the mechanical properties of hydrogels.[16–19] Thirdly, graphene hydrogels possess porous structure, large water absorption capacity and excellent biocompatibility, which makes graphene

Z. J. Fan, Prof. J. Q. Wang, P. W. Gong, L. M. Ma, Prof. S. R. Yang
State Key Laboratory of Solid Lubrication
Lanzhou Institute of Chemical Physics
Chinese Academy of Sciences
No. 18 Tianshui Middle Road
Lanzhou 730000, China
E-mail: jqwang@licp.cas.cn
Prof. B. Liu, S. Y. Zhang, Q. Q. Lin
School of Stomatology
Lanzhou University
Lanzhou 730000, China

DOI: 10.1002/adfm.201304202

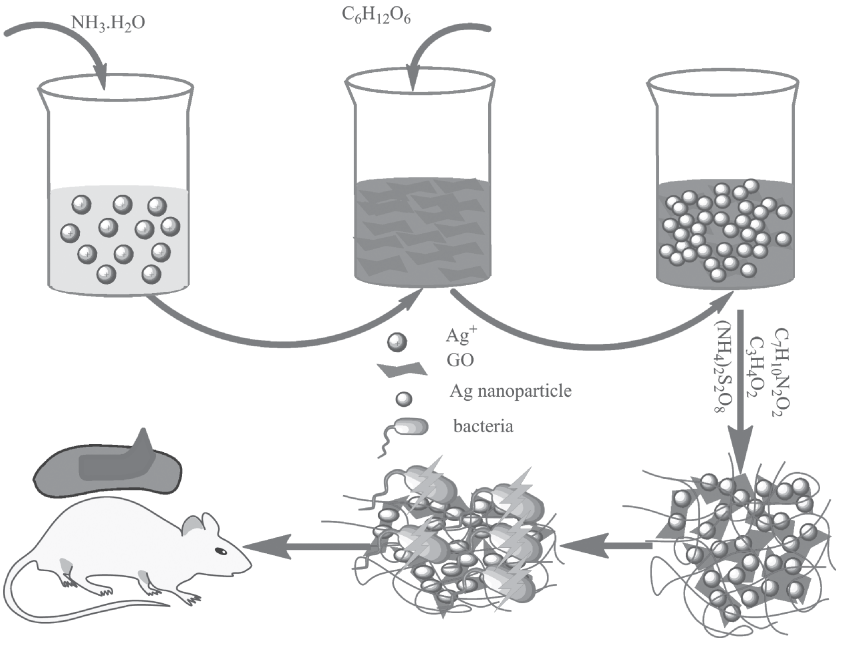

Figure 1. Illustration of the synthetic route of Ag–graphene and the corresponding hydrogel as a wound dressing.

hydrogels conductive to cellular adhesion and growth.[20–23] Fourthly, graphene hydrogels can maintain moist environment around wound thereby facilitating wound healing. So far, graphene hydrogels have been mainly used as cellular scaffolds, carriers of controlled drug release, biosensors, stimuli-responsive actuators, supercapacitors and catalytic bulk materials and etc.[24–28] Furthermore, to the best of our knowledge, no report is currently available about graphene hydrogels used in wound dressing. This research on the wound dressing based on graphene hydrogel will extend new application range of graphene in biomedicine. Based on the above mentioned advantages, it seems that graphene hydrogels should be an eligible candidate of wound dressing. However, some studies have pointed out that graphene does not have intrinsic bacteriostatic or antibacterial activity owing to its lack of antibacterial activity,[29,30] therefore such drawback limits its further application as the wound dressing.

In order to avoid wound infection caused by bacteria, some antibacterial agents must be incorporated into graphene hydrogel. Among various antimicrobial agents, silver is the most common and well-studied types of antimicrobial agents due to its wide spread antimicrobial spectrum.[31] Silver is reported to be effective against a wide range of aerobic, anaerobic, Gram positive, Gram negative, fungus and viruses.[32–34] Recently, there have been some reports about Ag–graphene nanocomposites. Faria. et al. synthesized Ag nanoparticles and graphene composite, and found this composite showed excellent antibacterial activity against the Gram-negative.[35] Kholmanov. et al. reported that graphene and Ag nanowires composite film possessed antibacterial properties with a potential application as biomedical devices.[36] Cai. et al. constructed polyethyleneimine-modified reduced graphene oxide and Ag composite, and found this composite had substantially higher antibacterial activity.[37] These studies sufficiently demonstrated that the introduction of Ag on the substrate of graphene can enhance the antibacterial performance of graphene. Almost all studies only used the powders or films of Ag–graphene composite as the antibacterial materials, but graphene hydrogels have not been referred. Therefore, in the present research we incorporate silver into graphene hydrogel, and hope to develop novel graphene hydrogel-based wound dressing with improved bacteria-killing and accelerated wound healing capabilities.

This paper reports the synthesis of Ag–graphene composites with different Ag to graphene mass ratios in the presence of glucose as a green reducing agent as well as the preparation of Ag–graphene hydrogels from Ag–graphene composites, acrylic acid (denoted as AA) and *N,N′*-methylene bisacrylamide (BIS) and antibacterial test and wound healing evaluation of as-obtained Ag–graphene composite hydrogels.

2. Result and Discussion

2.1. Characterization of GO and Ag–Graphene Composites

As illustrated in **Figure 1**, graphene hydrogel is synthesized with a two-step approach including the synthesis of Ag–graphene composites and the synthesis of corresponding hydrogels, where Ag–graphene composites were prepared with an environmentally friendly and facile method using glucose as the reductive agent.

Figure 2A presents the ultraviolet-visible light (UV-vis) absorption spectra of the aqueous dispersions GO and various Ag–graphene composites with different Ag to graphene mass ratios. GO shows two UV–vis absorption peaks at 232 nm and 300 nm, corresponding to π–π^* transitions of aromatic C = C bond and n–π^* transitions of C = O bond in GO.[38] The incorporation of Ag leads to absorption peaks around 400 nm whose intensity tends to gradually increase with the increase of Ag content (but the absorption peak of Ag0.5G1 (its Ag to graphene mass ratio is 0.5:1; those Ag–graphene composites with other Ag to graphene mass ratios are denoted in the same manner) is insignificant, due to too low dosage of Ag). These absorption peaks of Ag are attributed to surface plasmon resonance of colloidal silver, which indicates that Ag in various Ag–graphene composites exists in the state of nanoparticles.[39] The transmission electron microscopic (TEM) and high-resolution TEM (HRTEM) images of various Ag–graphene composites (Figure 2B–D) illustrate that Ag nanoparticles are homogeneously and densely attached onto the surface of graphene, and their size varies with varying Ag to graphene mass ratio. Namely, the average size of Ag nanoparticles increases from 11.5 nm to 39.0 nm when Ag to graphene mass ratio

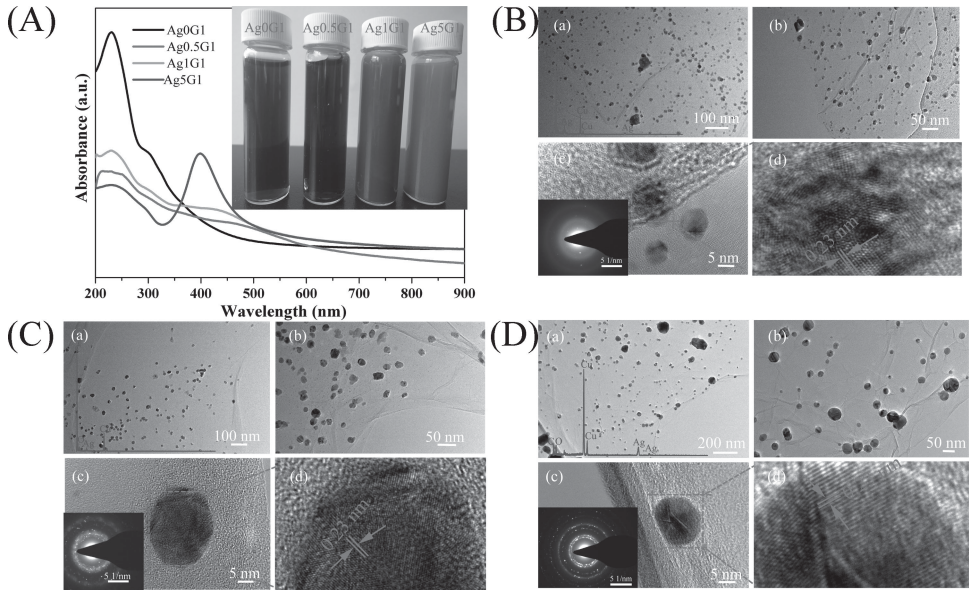

Figure 2. A) UV–vis absorption spectra of aqueous dispersions of Ag0G1, Ag0.5G1, Ag1G1, and Ag5G1. (Insets: the optical images of Ag0G1, Ag0.5G1, Ag1G1, and Ag5G1.) B) TEM images of Ag0.5G1, C) Ag1G1, and D) Ag5G1 with blue curves of EDX and insets of SAED.

rises from 0.5:1 to 5:1. This is because, as a carrier of Ag nanoparticles, graphene can prevent Ag nanoparticles from aggregating and help them to retain uniform dispersion on graphene surface. Corresponding energy-dispersive X-ray (EDX) analysis of three kinds of Ag/graphene composites confirms that Ag nanopaticles are present on the surface of graphene nanosheets (see blue curves in Figure 2); and relevant selected area electron diffraction (SAED) patterns of all Ag–graphene composites demonstrate that they belong to multiple crystals.[40] Moreover, the HRTEM images of Ag–graphene composites Ag0.5G1, Ag1G1, and Ag5G1 show clear lattice fringes with an interplanar distance of 0.23 nm, corresponding to the (111) plane of Ag.[41]

2.2. Characterization of Graphene and Ag–Graphene Hydrogels

Figure 3a shows the X-ray diffraction (XRD) patterns of GO and Ag–graphene composites. GO shows a typical diffraction peak at 9.8°, corresponding to the (002) diffraction peak of graphene oxide.[41] When aqueous ammonia is added into silver nitrate solution, silver ammonia complex $[Ag(NH_3)^{2+}]$ that can be easily attracted to negatively charged oxygen functional groups on GO is formed (Figure 1).[38] Upon addition of glucose, $[Ag(NH_3)^{2+}]$ can be reduced by the aldehyde groups of glucose to generate Ag nanoparticles, as evidenced by relevant XRD analysis (the four XRD peaks at 38.1°, 44.2°, 64.5°, and 77.5° correspond to the (111), (200), (220), and (311) diffractions of metallic Ag (JCPDS No. 04–0783)).[40–44] Similar incomplete reduction of GO by glucose yielding graphene is also reported elsewhere.[45] Particularly, Ag–graphene composite Ag5G1 does not show the XRD peak of GO at 9.8°, because it involves a larger amount of glucose and allows the complete reduction of $[Ag(NH_3)^{2+}]$ as compared with the other Ag–graphene composites of different Ag to graphene mass ratio.[45]

Figure 3b presents the X-ray photoelectron survey spectra (XPS) of GO and various Ag–graphene composites. GO shows only C and O XPS peaks, while Ag–graphene composites with different Ag to graphene mass ratios show the signals of Ag3d, Ag3p1, and Ag3p5.[46] Relevant high-resolution Ag3d XPS spectra (Figure 3c) contain two peaks at 368.4 eV and 374.4 eV, corresponding to Ag3d5/2 and Ag3d3/2, respectively.[47] In the meantime, the high-resolution C1s spectra (Figure 3d) illustrate that the intensities of all C1s peaks of carbon-oxygen bonds decline dramatically with the increase of Ag content, which indicates that GO is partially reduced by glucose.[47,48] Even so, the dispersibility of Ag–graphene composites is not affected by the reduction of GO, and hence they exhibit good dispersibility in aqueous solution (see the inset in Figure 2A). Of course, the partial reduction of GO in the present research is undesired, because it causes damage to the hydrophilicity of as-prepared Ag–graphene composites. Nevertheless, such a reductive process is unaviodable when any reductive agents are adopted to prapare Ag–graphene nanoparticles.

The Fourier transform infrared (FTIR) spectra of GO, Ag0.5G1, Ag1G1, and Ag5G1 are shown in Figure S1 (Supporting Information). GO shows FTIR absorption peaks at 3446, 1722, 1639, 1050 cm^{-1}, and they correspond to O–H stretching vibration, carbonyl (C = O) stretching vibration, C = C stretching vibration and C–O stretching vibration.[49] What is worth special notice is that the adsorption bands of the oxygenated functional groups in the three kinds of Ag–graphene composites are much weaker than those in GO,[45] which could be due to the partial reduction of GO by glucose during the synthesis of Ag–graphene nanocomposite.

Based on the successful preparation of Ag–graphene composites, Ag–graphene hydrogels were prepared by crosslinking of Ag–graphene composites with AA and BIS in the presence of APS as an initiator. Resultant Ag–graphene composite hydrogels exhibit gel-like structure, and in particular,

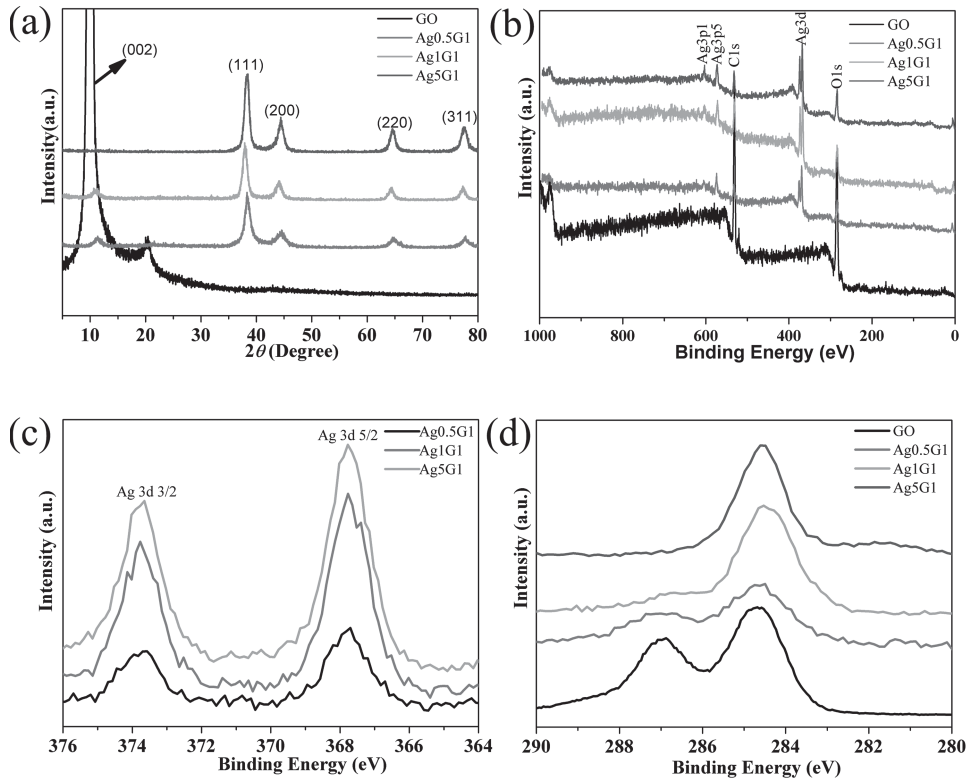

Figure 3. a) XRD patterns of Ag0G1, Ag0.5G1, Ag1G1, and Ag5G1; b) XPS spectra of Ag0G1, Ag0.5G1, Ag1G1, and Ag5G1; c) high-resolution Ag3d spectra of Ag0.5G1, Ag1G1, and Ag5G1; and d) high-resolution C1s spectra of Ag0G1, Ag0.5G1, Ag1G1, and Ag5G1.

the color of Ag5G1 hydrogel with a higher Ag concentration is different from that of Ag0.5G1 and Ag1G1 hydrogels (Supporting information Figure S2). Besides, the XRD patterns of GO and Ag–graphene hydrogels shown in Figure S3 indicate that Ag–graphene composite hydrogels retain the characteristic peaks of Ag at 38.1°, 44.2°, 64.5°, and 77.5°.[45]

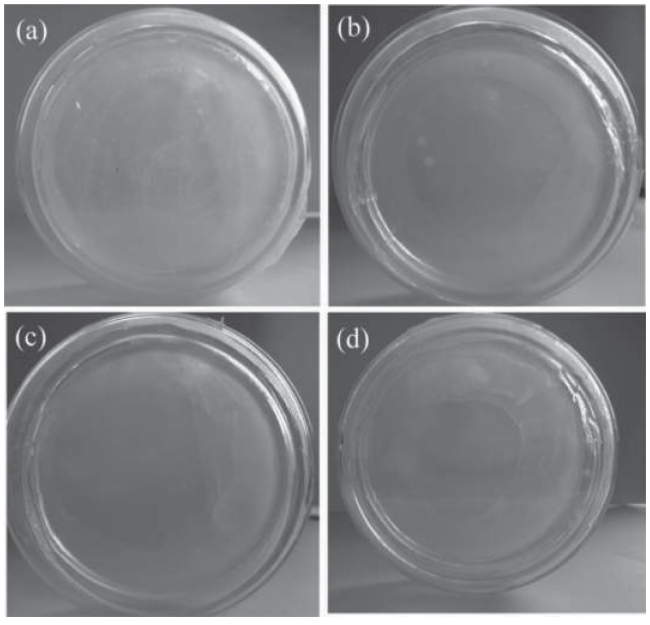

Figure 4. Photographs of bacterial colonies formed by E. coli cells treated with hydrogels of a) Ag0G1, b) Ag0.5G1, c) Ag1G1, and d) Ag5G1, respectively.

2.3. Antibacterial Performance

Bacterial infection is the main cause of wound infection, which means that the antibacterial activity of dressing should be evaluated before it is put into use for healing impaired wound. Thus the antibacterial activities of Ag0G1, Ag0.5G1, Ag1G1, and Ag5G1 hydrogels were determined by shaking flask method and disc diffusion method, respectively. **Figures 4**, **5** present the antibacterial activities of various hydrogels against Gram-negative *Escherichia coli* (denoted as E. Coli) and Gram-positive *Staphylococcus aureus* (denoted as S. Aureas) determined by shaking flask method. It can be seen that Ag0G1 exhibits poor antibacterial activity against E. coli and S. aureas (see Figures 4a, 5a), which is in aggrement with what is reported elsewhere.[39] Hydrogel Ag0.5G1 possesses much better antibacterial activity than Ag0G1 hydrogel, which is due to the incorporation of Ag nanoparticles, but its antibacterial effect is still unsatisfactory (see Figures 4b, 5b). After more Ag nanoparticles are incorporated, both Ag1G1 and Ag5G1 hydrogels exhibit much better antibacterial activity against E. Coli and S. aureas than Ag0.5G1 hydrogel (see Figure 4c,d). Namely, no E. coli colonies remain on the agar plate treated with both hydrogels; two S. aureas colonies (red circles) remain on the agar plate treated with Ag1G1 hydrogel, and no S. aureas colonies remain on the agar plate treated with Ag5G1 hydrogel. This means that Ag5G1 hydrogel

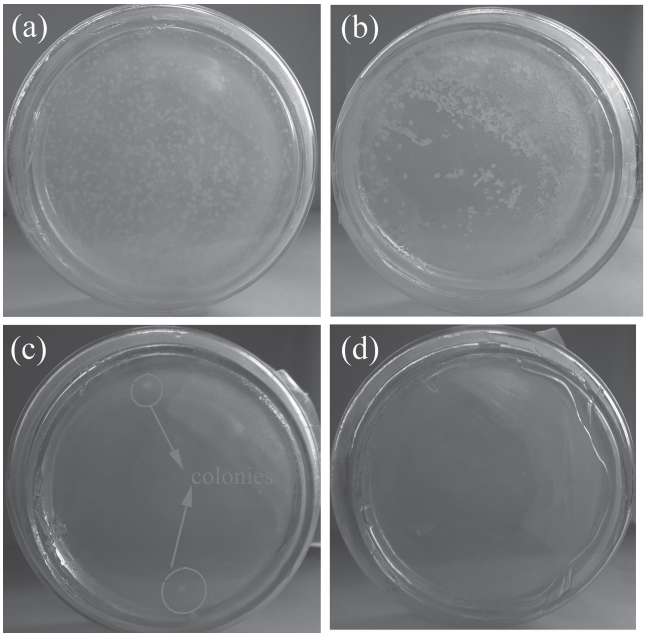

Figure 5. Photographs of bacterial colonies formed by S. aureas cells treated with hydrogels of a) Ag0G1, b) Ag0.5G1, c) Ag1G1, and d) Ag5G1, respectively.

with the highest content of Ag nanoparticles exhibits the best antibacterial activity against S. aureas among various Ag–graphene hydrogels under investigation.

In order to further examine the antibacterial effect of various as-prepared Ag–graphene composite hydrogels, we adopted disc diffusion method to evaluate their antibacterial performance. As shown in Figure S4, the inhibition zone diameters of Ag1G1 and Ag5G1 hydrogels are larger than those of Ag0G1 and Ag0.5G1 hydrogels, which indicates that Ag1G1 and Ag5G1 hydrogels exhibit better bacterial inactivation capability than Ag0G1 and Ag0.5G1 counterparts. This agrees well with what is observed with shaking flask method. Naturally, Ag0G1 hydrogel without Ag nanoparticles exhibits poor antibacterial activity, and the antibacterial activity of various Ag–graphene composite hydrogels tends to increase with increasing dosage of Ag nanoparticles, because Ag can inactivate microorganism cells by destroying the cell membrane and DNA replication ability.[42] Similar phenomenon was also observed by Yu et al. who reported that water-soluble Ag–graphene nanocomposite displays much better antibacterial performance than pure Ag nanoparticles or graphene, due to the synergistic interaction between graphene and Ag nanoparticles.[32] The possible reason may be that graphene can prevent Ag nanoparticles from aggregating, in addition, graphene has large surface areas, which can integrate more Ag nanoparticles onto its surface. Higher Ag loading on Ag5G1 hydrogel can obtain better antibacterial effect. In addition to the above mentioned several factors, and besides, the size of the Ag nanoparticles also has an important influence on the antibacterial effect of hydrogel.[32] Large size of the Ag nanoparticles contributes to enhance antibacterial activity.[32] Taking Ag5G1 hydrogel for example (Figure. 2B–D), larger size of Ag nanoparticles can get better antibacterial performance. Particularly, the better antibacterial effect of Ag1G1 and Ag5G1 hydrogels may refer to potentially better wound healing efficiency. Therefore, both Ag1G1 and Ag5G1 hydrogels are chosen to be further studied as follows.

2.4. Porous Structure of Hydrogels

It is well known that a porous structure is important for the supply of oxygen, absorption of exudates and maintance of large amount of water.[50] **Figure 6** shows the porous structure of various hydrogels observed with SEM. Obviously, Ag0G1 hydrogel contains few and closed pores (Figure 6a), and its size is smaller than that of Ag1G1 and Ag5G1 hydrogels. In comparison with Ag0G1 hydrogel, Ag1G1 and Ag5G1 hydrogels exhibit highly porous structure, and their pores are interconnected to form an "open-cell" structure (Figure 6b). Besides, the pore size of Ag5G1 hydrogel is larger than that of Ag1G1 hydrogel, and the former possesses the largest porous structure among various tested Ag–graphene composite hydrogels (Figure 6c), which indicates that Ag–graphene composite hydrogels containing a higher content of Ag nanoparticles can better facilitate the exchange of oxygen, maintain the suitable moisture environment and favour cellular adhesion and growth.

2.5. MTT (3-(4,5-Dimethyldiazol-2-yl)-2,5-Diphenyl Tetrazolium Bromide) Assay

Aside from good antibacterial activity, biocompatibility is another criterion to evaluate the feasibility of dressing in healing wound. Biocompatibility is often assessed by MTT assay that is commonly used to analyze the possible harmful effects induced in cells by materials, with which the cellular mitochondria activity upon exposure to materials is quantified.[51,52] For this purpose, Ag1G1 and Ag5G1 hydrogels with better antibacterial activity were selected as the experimental groups, and Ag0G1 hydrogel was selected as the control

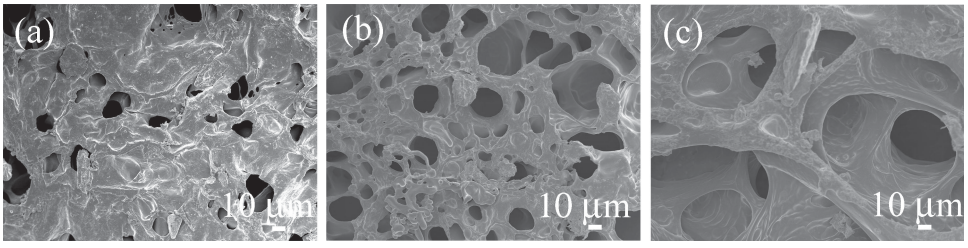

Figure 6. SEM images of a) Ag0G1, b) Ag1G1, and c) Ag5G1 hydrogels.

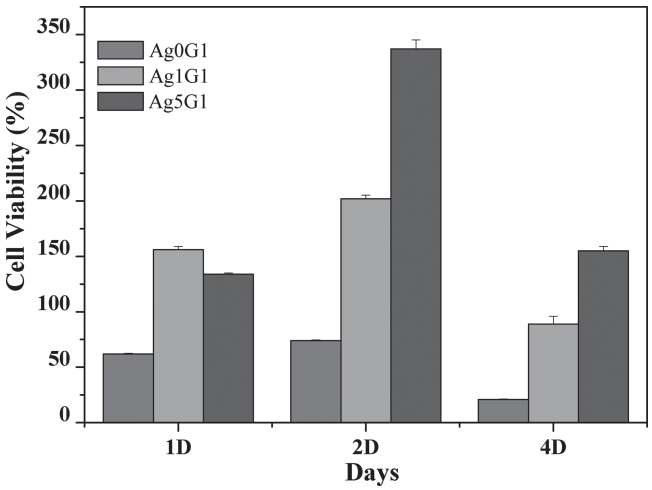

Figure 7. Cellular proliferation analysis, the cells were respectively incubated for 1, 2, and 4 days on the surfaces of Ag0G1, Ag1G1, and Ag5G1.

group, where L929 fibroblasts were seeded directly onto the surfaces of Ag0G1, Ag1G1, and Ag5G1 hydrogels. The tested cells were incubated for 1, 2, and 4 days, respectively, and then their viability and proliferation were assessed by MTT assay. As shown in **Figure 7**, the control group with poorer pore distribution exhibits lower cell viability than the experimental groups in different cultured periods. Namely, Ag5G1 hydrogel exhibits lower cell viability than Ag1G1 hydrogel in 1 day incubation, but it exhibits higher cell viability than Ag1G1 hydrogel in 2 day and 4 day incubations. Besides, the cell viability of the three groups tends to decrease to some extent in 4 day incubation, which is possibly due to lack of nutrition leading to death of partial cells. In one word, elevating Ag content causes negligible harmful effects to cell viability of Ag–graphene composite hydrogels, and the larger interconnected pores mainly account for the better cell viability of Ag5G1 hydrogel.

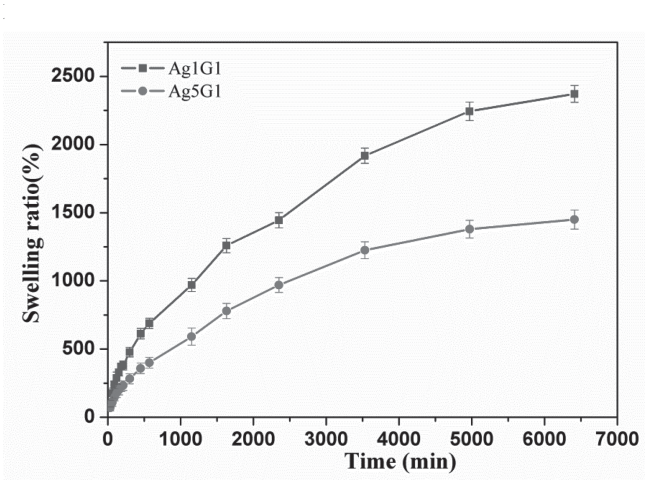

Figure 8. Swelling behaviors of Ag1G1 and Ag5G1 hydrogels soaked in SBF for different times.

2.6. Swelling Ratio

Hydrogel wound dressings should have large water absorption capacity in order to absorb wound exudates.[53] Thus Ag1G1 and Ag5G1 hydrogels with better antibacterial performance were soaked in simulated body solution (denoted as SBF) for different periods of time to evaluate water absorption capacity. As shown in **Figure 8**, the SBF absorbing capacity of both hydrogels increases with extending soaking time and reaches equilibrium after 100 h of soaking. This indicates that both hydrogels have large SBF absorption capacity, which is favorable for them to absorb a large amount of excessive exudates in a long duration. Besides, Ag1G1 hydrogel exhibits a higher swelling ratio than Ag5G1 hydrogel at all tested incubation periods, which could be because the reduction degree of graphene, the main water absorbing material, impacts the water absorbing capacity. As illustrated in Figure 3d, Ag5G1 hydrogel has a higher reduction degree of graphene than Ag1G1 hydrogel, therefore the former exhibits lower water absorbing capacity than the latter. Even so, the swelling ratio of Ag5G1 hydrogel containing partially reductive graphene and hydrophilic polyacrylic acid (1456%) is larger than that reported elsewhere (400% of the dressing based on polyvinyl alcohol and chitosan,[54] 900% of the dressing composed of chitosan and pectin,[55] and 959% of the dressing made of poly(glutamic acid) and chitosan).[56] In this sense, Ag5G1 hydrogel with a high enough swelling ratio meets with the requirement for effective absorption of exudates.

2.7. In-Vivo Wound Healing

Aside from antibacterial test and biocompatibility examination, in vivo experiment is indispensible for evaluating the real wound-healing effect of potential wound dressing. **Figure 9** shows the optical microscopic images of (1 cm × 1 cm) small wound cuts treated with Ag0G1, Ag1G1 and Ag5G1 hydrogels or left undressed (control group) for 5, 10, and 15 days. The control group and Ag0G1 hydrogel have no significant effects on the wound size after 5-day and 10-day treatments. Differing from the control group and Ag0G1 hydrogel, Ag1G1, and Ag5G1 hydorgels tested under the same conditions are able to reduce the wound size by 25% and 43%, respectively (**Figure 10**). After 15-day treatment with Ag0G1 hydrogel, the wound size is not reduced but instead enlarged, which is because Ag0G1 hydrogel exhibits few and closed pores thereby leading to poor air permeability and lack of oxygen. Since oxygen is necessary for supporting cellular and tissular growth, and the lack of oxygen may cause the death of cells and tissues, thus Ag0G1 hydrogel is unsuitable for wound healing. Moreover, some anaerobic bacteria can proliferate owing to lack of oxygen. As a result, Ag0G1 hydrogel without antibacterial effect even cannot kill anaerobic bacteria but causes severe inflammatory response thereby leading to deterioration and size-increase of the wound. To our delight, the size of the wound tends to decline after being treated by Ag1G1 and Ag5G1 hydrogels; and in particular, Ag5G1 hydrogel has a wound healing ratio of 98% (Figure 10), higher than that of Ag1G1 hydogel (85%) and the control group (53%). Such an excellent wound-healing effect of Ag5G1 hydrogel could be attributed to the synergistic effects

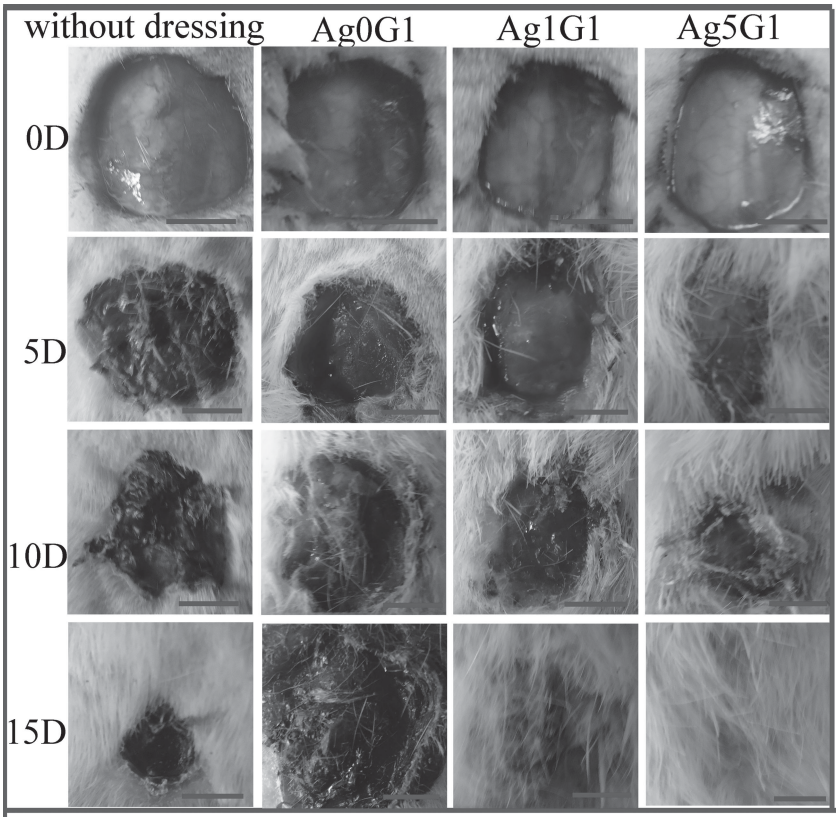

Figure 9. Visual observation of surface healing upon small wounds (scale bar = 0.5 cm).

between the antibacterial performance of Ag nanoparticles and the porous structure of graphene. Furthermore, Table S2 (Supporting Information) comparatively lists the wound healing ratio of various Ag–graphene composite hydrogels with those of other dressings reported elsewhere.[57–62] It can be seen that, although the dressings reported provide satisfactory wound healing ratios, they are less competitive as compared with Ag–graphene hydrogels. In one word, Ag5G1 hydrogel exhibits excellent wound-healing performance over a very short period and may find potential clinic applications.

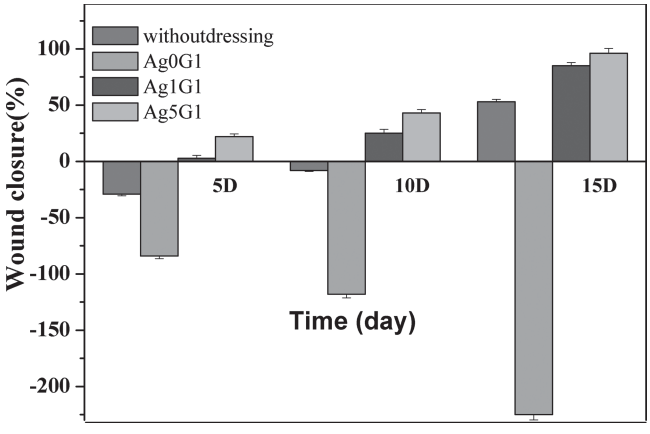

Figure 10. Wound closure untreated and treated with Ag0G1, Ag1G1 and Ag5G1. Values are mean ± SD for each group. (Negative values in the direction of the negative axis indicated the wound deteriorated and enlarged.)

2.8. Histological Analysis

Wound healing is a specific biological process related to the general phenomenon of growth and tissue regeneration, and it can be divided into four phases, including haemostasis, inflammation, migration, proliferation, and maturation phases.[63] Hematoxylin and eosin stained sections (H&E staining) were employed in the present research to evaluate the wound healing progress. As shown in **Figure 11**, a number of inflammatory cells emerge on the wound after 5-day treatments with the control group as well as Ag0G1 and Ag1G1 dressings, while some collagen fibers, fibroblasts and immature glandular cavity appear on the wound treated with Ag5G1 dressing for 5 days. Particularly, the collagen fibers and fibroblasts begin to migrate into injured area after 5-day treatment with Ag5G1 dressing, which corresponds to the migration phase of healing process and indicates that Ag5G1 dressing facilitates a quicker wound healing process than the other groups. After 10-day treatments, more inflammatory cells appear on the untreated wound and the one treated with Ag0G1 dressing, but much less inflammatory cells remain on the wound treated with Ag1G1 dressing for 10 days. Besides, 10-day treatment with the control group as well as Ag0G1 and Ag1G1 dressings yields a large number of microvessels, while treatment with Ag5G1 dressing under the same conditions generates mature glands grown from the glandular cavity. After 15-day treatments, the wound treated with Ag0G1 dressing is still dominated by acute inflammatory response, which well corresponds to its poor wound-healing effect and increased size of wound as well. In contrast, inflammatory cells disappear from the untreated wound and the one treated with Ag1G1 dressing for 15 days; and the untreated wound and the one treated with Ag1G1 dressing are covered by incomplete and thin epidermis. After being treated by Ag5G1 dressing, a complete and thickened epidermis is observed on the wound. Thus it can be concluded that Ag5G1 dressing exhibits the best wound-healing effect among various as-prepared Ag–graphene composite hydrogels.

2.9. Mechanical Properties

Although Ag5G1 hydrogel shows excellent wound-healing effect, its direct use as a wound dressing strongly relies on its mechanical properties, because skin is a motorial tissue whose mechanical properties change dynamically with various factors. Thus the tensile strength and the elongation at break of Ag5G1 hydrogel with the best wound-healing effect were measured by

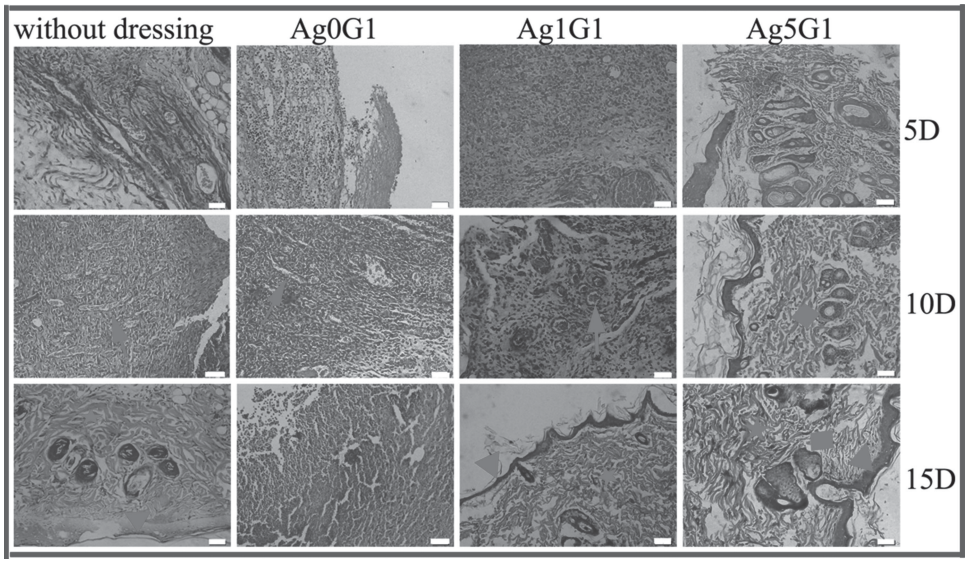

Figure 11. Photomicrographs showing section of skin tissues with H&E staining. Where quadrangle, arrow, triangle, and star respectively indicated gland, blood vessel, epidermis, and collagen fibers.

stretch test. As shown in Figure S5a,b (Supporting Information), Ag5G1 hydrogel is very ductile, and it can be folded four times or knotted. Namely, it exhibits a tensile strength of about 102 kPa and an elongation at break of about 222%, respectively (Figure S5c, Supporting Information), and it is much superior to the hydrogel composed of AA and BIS without graphene (tensile strength: about 3 kPa; elongation at break: 70%).[64] This means that introducing graphene helps to significantly improve the mechanical properties of Ag–graphene hydrogel thereby adding to the application of Ag–graphene hydrogel for wound dressing under high stresses.

3. Conclusions

A series of Ag–graphene composite hydrogels have been prepared by crosslinking Ag/graphene composites with acrylic acid and N,N′-methylene bisacrylamide in the presence of glucose as a green reducing agent which is favorable for minimizing the toxicity effect on the tissues. It has been found that Ag5G1 composite hydrogel with a Ag to graphene mass ratio of 5:1 exhibits desired antibacterial abilities aganist both Gram-negative Escherichia coli and Gram-positive Staphylococcus aureus. Although Ag5G1 hydrogel contained more Ag than others, there was a negligible effect on the fibroblastic biocompatibility. In comparison with some reported hydrogels with high swelling ratio, higher swelling ratio can be achieved for the Ag5G1 hydrogel owing to the existence of partially reductive graphene and hydrophilic polyacrylic acid. Meanwhile, graphene embedded in hydrogel can enhance the tensile strength and elongation at break of hydrogel, and fit the mechanical necessary of dressing. When this hydrogel was used to cure full-thickness skin wound, a higher wound healing ratio in less time can be observed compared to other hydrogels and some reported dressings, and this result was further proved by histological analysis, demonstrating its potential application in wound treatment. However, future pre-clinical and clinical studies are recommended to provide evidence-based medicinal findings regarding the routine application of Ag5G1 hydrogel as wound dressings in clinical.

4. Experimental Section

Materials: Graphite powders and D-glucose were purchased from Shanghai Chemical Co., Ltd. $AgNO_3$ was purchased from Tianjin No.2 Chemical Reagent Factory. $(NH_4)_2S_2O_8$ (denoted as APS) was obtained from Tianjin No.1 Chemical Reagent Factory. AA was obtained from Shanghai Shanpu Chemical Co., Ltd. BIS was purchased from Shanghai Zhongxin Chemical Reagent Co., Ltd. $NH_3{\cdot}H_2O$ (28%) was purchased from Baiyin Liangyou Chemical Reagent Co., Ltd. Dimethyl sulfoxide (DMSO) and Dulbecco's modified Eagle's medium (DMEM) were purchased from Gibco. Trypsin-EDTA (EDTA refers to ethylenedimiane tetraacid) solution and 3-(4,5-dimethyldiazol-2-yl)-2,5-diphenyl tetrazolium bromide (MTT, guaranteed reagent) were supplied by Sigma. Fibroblastic cells (L929) were provided by the Fourth Military Medical University. Ultrapure water (>18 MΩ cm) was used for rinsing and as the solvent as well.

Preparation of Ag–Graphene Nanocomposite with Different Ag Contents: GO colloid solution was prepared from graphite according to the modified Hummers method.[65] The final concentration of the solution is 2.5 mg mL^{-1}. The composites with different Ag/graphene weight ratio (0.5, 1 and 5) are denoted as Ag0.5G1, Ag1G1 and Ag5G1, respectively. The composites were synthesized according to the method of Xu et al.[66] The detailed reactive conditions are listed in Table S1 (Supporting Information). For example, Ag0.5G1 was synthesized according to the following experimental procedure: 0.55 mol L^{-1} $NH_3{\cdot}H_2O$ was obtained by adding 1.25 mL $NH_3{\cdot}H_2O$ (28%) to 50 mL H_2O solution. Resultant solution was slowly added to $AgNO_3$ solution until precipitate disappeared affording $Ag(NH_3)_2OH$ solution. Into as-obtained $Ag(NH_3)_2OH$ solution was poured 40 mL GO solution under magnetic stirring, followed by heating at 60 °C for 30 min and addition of 10 mL glucose solution (0.03 mol L^{-1}) under 1 h of disturbance to afford a stable dispersion. Into resultant stable dispersion was added sodium

chloride electrolyte, and then the mixed dispersion was washed with water repeatedly to provide desired Ag0.5G1 composite. Composites Ag1G1 and Ag5G1 were prepared in the same manners while reactive conditions were changed.

Synthesis of Ag–Graphene Composite Hydrogel Crosslinked by AA and BIS: The composite hydrogels were prepared by in situ polymerization of monomer AA and crosslinkable monomer BIS in the presence of APS as an initiator. In this study, four composite hydrogels, including Ag0G1 (graphene oxide hydrogel without Ag), Ag0.5G1, Ag1G1, and Ag5G1 were synthesized by modified Ye method.[64] Briefly, 4 mL AA, 0.04 g BIS and 0.04 g APS were added to 40 mL GO or Ag–graphene dispersion (2 mg mL^{-1}) and stirred for 30 min in an ice-water bath to afford a dispersion. The dispersion was poured into a petri-dish with a diameter of 10 cm, and then the petri-dish was put into an oven to allow further polymerization at 65 °C for 4 h. Upon completion of polymerization, the hydrogels were peeled from petri-dish and washed with water to remove impurities.

Characterization: The morphology of as-synthesized samples was observed with a scanning electron microscope (SEM, JEOL JSM–6701F) and a transmission electron microscope (TEM, JEOLJEM–2010). The structure and phase composition of as-synthesized samples were characterized by X-ray diffraction (XRD, Rigaku D/Max–2400 diffractometer, Cu $K\alpha$ radiation and graphite monochrometer, λ = 1.54056 Å), Fourier transform infrared spectrometry (FTIR, Bruker IFS66V FTIR spectrometer), and X-ray photoelectron spectroscopy (XPS, PHI–5702, Physical Electronics, USA; monochromated Al Kα irradiation with chamber pressure of 3×10^{-8} Torr under testing conditions), respectively.

Antibacterial Measurement: Shaking flask method[67] and disc diffusion method[68] were applied to detect the antibacterial performance of Ag–graphene composite hydrogels. Two kinds of strains, E. coli and S. aureus, were inoculated in Luria Bertani medium and cultured at 37 °C for 12 h on a rotary shaker at 200 rev min^{-1}. Two strains were harvested by centrifugation and diluted to 10^5–10^6 CFU mL^{-1} with a sterile phosphate saline buffer solution (PBS) while all the conditions were kept sterile. The experimental process for shaking flask method is described as follows: the samples of Ag0G1, Ag0.5G1, Ag1G1, and Ag5G1 were cut into discs with the diameter of 1 cm and then put into flasks with 10 mL bacteria suspension (10^5–10^6 CFU mL^{-1}), respectively. The flasks were held in a shaking table at 37 °C for 30 min, then 100 µL of the suspension was taken out and mixed with 20 mL of agar culture medium. After solidification of culture medium, the plates were turned over and incubated for 12 h to form colony units. Three parallel samples were adopted for each experimental group so as to ensure the correction of experimental results. Disc diffusion method is a commonly used method.[69,70] Ag5G1 hydrogel with excellent antibacterial activity was adopted for the following experiments.

Fibroblastic Cells Culture: L929 cells were employed to evaluate the biocompatibility of as- prepared hydrogels. The fibroblastic cells were grown in Dulbecco's modified Eagle medium containing 10% fetal bovine serum, 2 mM L-glutamine, 4.5 g L^{-1} glucose, and 1% antibiotic/antimycotic solution. The cells were kept under aseptic conditions at 37 °C and 5% CO_2. The media were refreshed every 2 days until the cells reached confluence.

Cellular Viability by Tetrazolium Dye MTT Assay: The MTT assay, which is used for determining cell viability, is based on the reductive cleavage of MTT (a yellow salt) to formazan (a purple compound) by mitochondrial dehydrogenase of living cells.[71] To-be-tested Ag–graphene hydrogels were cut into 1 cm diameter of discs. All discs of various hydrogels were sterilized in 75% ethanol for 30 min and irradiated in ultraviolet (UV) radiation for another 30 min. The discs were rinsed with sterilized PBS (10 mM, pH 7.4) thrice and then placed into a 24-well plate and seeded with 1 mL cell suspension at 2×10^4 cells mL^{-1} concentration on each well. At a pre-set time (1, 2, or 4 days), 100 µL MTT solution was injected into each well, and then the cells were cultured for another 4 h. Upon completion of culturing, the upper solvent was discarded, and the blue formazan reaction product was dissolved by adding 200 µL of DMSO. Resultant dissolvable solution was transferred into a 96-well plate, and then its absorbance was recorded with a microplate reader. The data of three parallel experiments were averaged.

Blank and control groups were established to calibrate the cellular survival rate. For this purpose, only the culture media were added to the blank group, whereas cells and culture media without samples were added to the control group. The measured optical density (OD) values of the blank, control, and experimental groups are coded as ODbla, ODcon, and Odexp; and the cellular survival rates are calculated as

$$\text{Survival Rate} = \frac{OD_{exp} - OD_{bla}}{OD_{con} - OD_{bla}} \times 100\%$$

Results are expressed as mean ± standard deviation and are analyzed with the Student's t-test.

Simulated Body Fluid (SBF) Absorption Rate: The SBF absorbing capacity (SAC) of a wound dressing is a key design criterion for providing and maintaining a moist environment over the wound bed. SBF was prepared in laboratory according to the procedure for preparing Kokubo's solution while the ionic concentration was kept similar to that of human blood plasma.[72,73] Various hydrogels were cut into discs with the diameter of 1 cm and were dried at 60 °C for 2 h in an oven. The dried sample (Wd) was immersed in SBF and maintained at 37 °C. At specific intervals of time, the samples were taken out and weighed (Ws). The SAC is calculated as[74]

$$\text{SAC}\ (\%) = \frac{Ws - Wd}{Wd}$$

In Vivo Wound Healing: The wound healing characteristics of various as-prepared hydrogels were evaluated using a rat model. All experiments were performed with the approval of the Institute's Animal Ethics Committee, and male, Sprague Dawley rats weighing approximately 250 g were employed to evaluate the wound healing characteristics. The dorsal hair of rats was shaved and the animals were anesthetized by intraperitoneal injection of urethane at a dose of 2 mg kg^{-1} body weight. One full thickness skin wound of 1 cm^2 area was prepared by excising the dorsum of the animals. The excised wounds were covered with to-be-tested hydrogels (1.5 cm × 1.5 cm) and fixed with elastic adhesive bandage. Upon completion of wound-healing experiments, the animals were sacrificed by excess diethyl ether on 5, 10, and 15 days after surgery. The wounds were grossly examined and photographed for measurement of wound size reduction. Particularly, the dissected wound was not sterilized and the tested animals were kept under environmental conditions so as to avoid antibacterial interference caused by external conditions. As to histological analysis, the skin including the entire wound with adjacent normal skin was excised and fixed in 4% buffered paraformaldehyde. The wound sizes measured at the time of surgery and at the time of biopsy were used to calculate the percent reduction in wound size:[75]

$$\text{Wound size reduction}\ (\%) = \frac{[A_0 - A_t]}{A_0} \times 100$$

where A_0 and A_t are the initial wound area and wound area at a time interval "t", respectively.

Histology: Skins including the entire wound with adjacent normal skin fixed in 4% buffered paraformaldehyde were processed and embedded in paraffin, and sections of 3–5 µm were stained with hematoxylin and eosin.

Mechanical Properties: The tensile strength and the elongation at break of Ag5G1 hydrogel were determined with a Universal Testing Machine (AGS-X 5 KN, Shimadzu, Japan) under a temperature of 25 °C, a relative humidity of 25%, and a stretch speed of 20 mm min^{-1}.

Acknowledgements

The authors thank the National Natural Science Foundation of China (Grant Nos. 51205385 and 51075384) and "Top Hundred Talents Program" of Chinese Academy of Sciences for financial support.

Received: December 18, 2013
Revised: February 2, 2014
Published online: March 17, 2014

[1] X. Huang, Y. Zhang, X. Zhang, L. Xu, X. Chen, S. Wei, *Mater. Sci. Eng. C* **2013**, *33*, 4816.
[2] J. Grzybowski, M. K. Janiak, E. Oidak, K. Lasocki, J. Wrembel-Wargocka, A. Cheda, M. Antos-Bielska, Z. Pojda, *Int. J. Pharm.* **1999**,*184*, 179.
[3] C. Gong, Q. Wu, Y. Wang, D. Zhang, F. Luo, X. Zhao, Y. Wei, Z. Qian, *Biomaterials* **2013**, *34*, 6377.
[4] C. Radhakumary, M. Antonty, K. Sreenivasan, *Carbohydr. Polym.* **2011**, *83*, 705.
[5] G. D. Winter, *Nature* **1963**, *200*, 378.
[6] G. D. Winter, *Nature* **1962**, *193*, 293.
[7] M. Kokabi, M. Sirousazar, Z. M. Hassan, *Eur. Polym. J.* **2007**, *43*, 773.
[8] J. S. Gonzalez, L. N. Ludueña, A. Ponce, V. A. Alvarez, *Mater. Sci. Eng. C* **2014**, *34*, 54.
[9] Z. Tai, J. Yang, Y. Qi, X. Yan, Q. Xue, *RSC Adv.* **2013**, *3*, 12751.
[10] S. S. Roy, M. S. Arnold, *Adv. Funct. Mater.* **2013**, *23*, 3638.
[11] M. Yoonessi, Y. Shi, D. A. Scheiman, M. L. Colon, D. M. Tigelaar, R. A. Weiss, M. A. Meador, *ACS Nano* **2012**, *9*, 7644.
[12] A. A. Balandin, S. Ghosh, W. Bao, I. Calizo, D. Teweldebrhan, F. Miao, C. N. Lau, *Nano Lett.* **2008**, *8*, 902.
[13] A. M. Pintoa, I. C. Gonçalves, F. D. Magalhães, *Colloid Surf. B* **2013**, *111*, 188.
[14] K. Ai, Y. Liu, L. Lu, X. Cheng, L. Huo, *J. Mater. Chem.* **2011**, *21*, 3365.
[15] H. P. Cong, X. C. Ren, P. Wang, S. H. Yu, *Sci. Rep.* **2012**, *2*, 1.
[16] K. W. Putz, O. C. Compton, M. J. Palmeri, S. T. Nguyen, L. C. Brinson, *Adv. Funct. Mater.* **2010**, *20*, 3322.
[17] O. C. Compton, S. W. Cranford, K. W. Putz, Z. An, L. C. Brinson, M. J. Buehler, S. T. Nguyen, *ACS Nano* **2012**, *6*, 2008.
[18] J. R. Pottsa, D. R. Dreyerb, C. W. Bielawski, R. S. Ruoff, *Polymer.* **2011**, *52*, 5.
[19] H. P. Cong, P. Wang, S. H. Yu, *Small* **2014**, *10,* 448.
[20] S. Das, F. Irin, L. Ma, S. K. Bhattacharia, R. C. Hedden, M. J. Green, *ACS Appl. Mater. Interfaces* **2013**, *5*, 8633.
[21] H. P. Cong, P. Wang, S. H. Yu, *Chem. Mater.* **2013**, *25*, 3357.
[22] W. Li, J. Wang, J. Ren, X. Qu, *Adv. Mater.* **2013**, *25*, 6737.
[23] J. Lu, Y. S. He, C. Cheng, Y. Wang, L. Qiu, D. Li, D. Zou, *Adv. Funct. Mater.* **2013**, *23*, 3494.
[24] H. N. Lim, N. M. Huang, S. S. Lim, I. Harrison, C. H. Chia, *Int. J. Nanomed.* **2011**, *6*, 1817.
[25] Y. Zhao, L. Song, Z. Zhang, L. Qu, *Energy Environ. Sci.* **2013**, *6*, 352.
[26] R. Liu, S. Liang, X. Z. Tang, D. Yan, X. Li, Z. Z. Yu, *J. Mater. Chem.* **2012**, *22*, 14160.
[27] D. Ma, L. M. Zhang, *Mater. Sci. Eng. C* **2013**, *33*, 2632.
[28] Y. Xu, Z. Lin, X. Huang, Y. Liu, Y. Huang, X. Duan, *ACS Nano* **2013**, *7*, 4042.
[29] O. N. Ruiz, K. A. S. Fernando, B. Wang, N. A. Brown, P. G. Luo, N. D. McNamara, M. Vangsness, Y. P. Sun, C. E. Bunker, *ACS Nano* **2011**, *5*, 8100.
[30] J. Ma, J. Zhang, Z. Xiong, Y. Yong, X. S. Zhao, *J. Mater. Chem.* **2011**, *21*, 3350.
[31] M. Miraftab, R. Masood, V. Edward-Jones, *Carbohyd. Polym.* **2014**, *101*, 1184.
[32] W. P. Xu, L. C. Zhang, J. P. Li, Y. Lu, H. H. Li, Y. N. Ma, W. D. Wang, S. H. Yu, *J. Mater. Chem.* **2011**, *21*, 4593.
[33] N. Rangelova, L. Aleksandrov, T. Angelova, N. Georgieva, R. Müller, *Carbohyd. Polym.* **2014**, *101*, 1166.
[34] T. Angelovaa, N. Rangelovab, R. Yuryevc, N. Georgievaa, R. Müller, *Mater. Sci. Eng. C* **2012**, *32*, 1241.
[35] A. F. Faria, D. S. T. Martinez, S. M. M. Meira, A. C. M. M. A. Brandelli, A. G. S. Filho, O. L. Alves, *Colloid. Surf. B* **2014**, *113*, 115.
[36] I. N. Kholmanov, M. D. Stoller, J. Edgeworth, W. H. Lee, H. Li, J. Lee, C. Barnhart, J. R. Potts, R. Piner, D. Akinwande, J. E. Barrick, R. S. Ruoff, *ACS Nano* **2012**, *6*, 5157.
[37] X. Cai, M. Lin, S. Tan, W. Mai, Y. Zhang, Z. Liang, Z. Lin, X. Zhang, *Carbon* **2012**, *50*, 3407.
[38] S. Chook, C. Chia, S. Zakaria, M. Ayob, K. Chee, N. Huang, M. H. Neoh, H. N. Lim, R. Jamal, R. Rahman, *Nanoscale Res. Lett.* **2012**, *7*, 541.
[39] J. Li, C. Y. Liu, *Eur. J. Inorg. Chem.* **2010**, *2010*, 1244.
[40] J. Shen, T. Li, M. Shi, N. Li, Ye. M, *Mater. Sci. Eng. C* **2012**, *32*, 2042.
[41] J. Ma, J. Zhang, Z. Xiong, Y. Yong, X. S. Zhao, *J. Mater. Chem.* **2011**, *21*, 3350.
[42] S. You, S. M. Luzan, T. Szabó, A. V. Talyzin, *Carbon* **2013**, *52*, 171–180.
[43] Z. Zhang, J. Zhang, B. Zhang, J. Tang, *Nanoscale* **2013**, *5*, 118.
[44] S. K. Li, Y. X. Yan, J. L. Wang, S. H. Yu, *Nanoscale* **2013**, *5*, 12616.
[45] O. Akhavan, E. Ghaderi, S. Aghayee, Y. Fereydooni, A. Talebi, *J. Am. Chem. Soc.* **2012**, *22*, 13773.
[46] B. Jiang, C. Tian, G. Song, W. Chang, G. Wang, Q. Wu, H. G. Fu, *J. Mater. Chem.* **2012**, *48*, 1980.
[47] W. Yuan, Y. Gu, L. Li, *Appl. Surf. Sci.* **2012**, *261*, 753.
[48] L. Zheng, G. Zhang, M. Zhang, S. Guo, Z. H. Liu, *J. Power Sources* **2012**, *201*, 376.
[49] K. J. Huang, D. J. Niu, J. Y. Sun, C. H. Han, Z. W. Wu, Y. L. Li, X. Q. Xiong, *Colloid. Surf. B.* **2011**, *82*, 543.
[50] M. Wang, L. Xu, H. Hu, M. Zhai, J. Peng, Y. Nho, J. Q. Li, *Nucl. Instr. Meth. B* **2007**, *265*, 385.
[51] F. M. Young, W. Phungtamdet, B. J. S. Sanderson, *Toxicol. In Vitro* **2005**, *19*, 1051.
[52] Z. J. Fan, J. Q. Wang, Z. F. Wang, H. Q. Ran, Y. Li, L. Y. Niu, P. W. Gong, B. Liu, S. H. Yang, *Carbon* **2014**, *66*, 407.
[53] T. Wang, X. K. Zhu, X. T. Xue, D. Y. Wu, *Carbohydr. Polym.* **2012**, *88*, 75.
[54] J. H. Sung, M. R. Hwang, J. O. Kim, J. H. Lee, Y. I. Kim, J. H. Kim, W. S. Lyoo, S. S. Han, S. K. Ku, C. S. Yong, H. G. Choi, *Int. J. Pharm.* **2010**, *392*, 232–240.
[55] D. Archana, J. Dutta, PK. Dutta, *Int. J. Biol. Macromol.* **2013**, *57*, 193.
[56] C. T. Tsao, C. H. Chang, Y. Y. Lin, M. F. Wu, J. L. Wang, T. H. Young, J. L. Han, K. H. Hsieh, *Carbohydr. Polym.* **2011**, *84*, 812.
[57] B. Balakrishnan, M. Mohanty, P. R. Umashankar, A. Jayakrishnan, *Biomaterials* **2005**, *26*, 6335.
[58] S. H. Chen, C. T. Tsao, C. H. Chang, Y. T. Lai, M. F. Wu, C. N. Chuang, H. C. Chou, C. K. Wang, K. H. Hsieh, *Mater. Sci. Eng. C* **2013**, *33*, 2584.
[59] W. Wu, J. Shen, P. Banerjee, S. Zhou, *Biomaterials* **2011**, *32*, 598.
[60] D. Archana, B. K. Singh, J. Dutta, P. K. Dutta, *Carbohydr. Polym.* **2013**, *95*, 530.
[61] M. H Huang, M. C. Yang, *Int. J. Pharm.* **2008**, *346*, 38.
[62] J. S. Boateng, K. H. Matthews, H. N. Stevens, G. M. Eccleston, *Int. J. Pharm.* **2008**, *97*, 2892.
[63] C. C. Yates, D. Whaley, R. Babu, J. Zhang, P. Krishna, E. Beckman, A. W. Pasculle, A. Wells, *Biomaterials* **2007**, *28*, 3977.

[64] J. Shen, B. Yan, T. Li, Y. Long, N. Li, M. Ye, *Soft Matter* **2012**, *8*, 1831.
[65] Z. F. Wang, J. Q. Wang, P. L. Zhang, P. W. Gong, X. H. Liu, L. B. Zhang, J. F. Ren, H. G. Wang, S. R. Yang, *Carbon* **2012**, *50*, 5403.
[66] C. Xu, X. Wang, *Small* **2009**, *5*, 2212.
[67] Y. Wang, X. Xue, H. Yang, C. Luan, *Appl. Surf. Sci.* **2013**, *292*, 608.
[68] T. Bala, G. Armstrong, F. Laffir, R. Thornton, *J. Colloid. Interf. Sci.* **2011**, *356*, 395.
[69] Y. Liu, H. I. Kim, *Carbohydr. Polym.* **2012**, *89*, 111.
[70] M. Y. Murali, K. Vimala, V. Thomas, K. Varaprasad, B. Sreedhar, S. K. Bajpai, R. K. Mohana, *J. Colloid. Interf. Sci.* **2010**, *342*, 73.
[71] T. J. Wu, H. H. Huang, C. W. Lan, C. H. Lin, F. Y. Hsu, Y. J. Wang, *Biomaterials* **2004**, *25*, 651.
[72] T. Kokubo, H. Kushitani, S. Sakka, T. Kitsugi, T. Yamamuro, *J. Biomed. Mater. Res.* **1990**, *24*, 721.
[73] Z. J. Fan, J. Q. Wang, Z. F. Wang, Z. P. Li, Y. N. Qiu, H. G. Wang, S. H. Yang, *J. Phys. Chem. C.* **2013**, *117*, 10375.
[74] Ž. Jovanović, A. Krklješ, J. Stojkovska, S. Tomić, B. Obradović, V. Mišković-Stanković, Z. Kaćarević-Popović, *Radiat. Phys. Chem.* **2011**, *80*, 1208.
[75] S. H. Chen, C. T. Tsao, C. H. Chang, Y. T. Lai, M. F. Wu, C. N. Chuang, H. C. Chou, C. K. Wang, K. H. Hsieh, *Mater. Sci. Eng. C* **2013**, *33*, 2584.